A critical review of existing criteria for the prediction of pyrochlore formation and stability.

Antonio F. Fuentes[a], Sagrario M. Montemayor[b], Miroslaw Maczka[c], Maik Lang[d], Rodney C. Ewing[e] and Ulises Amador[f].*

[a] Cinvestav Unidad Saltillo, Apartado Postal 663, 25900 Ramos Arizpe, Coahuila, Mexico.

[b] Centro de Investigación en Química Aplicada, 25294 Saltillo, Coahuila, Mexico

[c] Institute of Low Temperature and Structure Research, Polish Academy of Sciences, P.O. Box 1410, 50-950 Wroclaw, Poland

[d] Department of Nuclear Engineering, University of Tennessee, Knoxville, TN 37996, USA

[e] Department of Geological Sciences, Stanford University, Stanford, CA 94305, USA

[f] Universidad San Pablo-CEU, CEU Universities, Facultad de Farmacia, Departamento de Química, Urbanización Montepríncipe, Boadilla del Monte, E-28668, Madrid, Spain

ABSTRACT

Depending on intrinsic (e.g. radius ratio rule r_{Ln}/r_{Zr}) and extrinsic factors (e.g. processing conditions), pyrochlore-type $Ln_2Zr_2O_7$ oxides achieve variable degrees of structural disorder. We

report on a systematic study of the structural and microstructural characteristics of the $Gd_{2-x}Ln_xZr_2O_7$ system, exploring the effect of replacing Gd with a wide range of homovalent lanthanide ions (Ln = Nd, Sm, Dy, Ho, Y, and Er; x = 0.20 and 0.80). All compositions were prepared via a mechano-chemical reaction between the corresponding oxides and characterized by X-ray diffraction (standard and synchrotron sources) using the Rietveld method, as well as by Raman spectroscopy. Irrespective of chemical composition, this study reveals that all compositions exhibit a fluorite-like structure. Furthermore, by firing each sample at 800 and 1400°C, we are able to analyze the transition to pyrochlore-like structures, featuring different degrees of disorder, in all but $Gd_{1.20}Y_{0.80}Zr_2O_7$, which retains the fluorite structure even after heating. The structural data are used to assess the existing criteria for predicting the formation and stability of the pyrochlore structure; according to this analysis, the simple radius ratio rule (r_{Ln}/r_{Zr}), provides a useful and sufficiently robust criterion. Because the pyrochlore structure has a strong tendency to disorder, it is not possible to define an empirical index similar to the Goldschmidt tolerance factor for perovskite.

KEYWORDS: Pyrochlore, fluorite structure, structure prediction, mechanical milling, Raman spectroscopy

INTRODUCTION

Lanthanide zirconates $Ln_2Zr_2O_7$ that adopt the pyrochlore structure exhibit a wide range of chemical and physical properties of interest for fundamental science and with important

technological applications.[1-5] Some of these properties are significantly altered by structural defects and disorder, which can be easily induced by temperature, pressure or irradiation. Therefore, intense research efforts are still aimed towards identifying and understanding the prevailing ordering/disordering mechanisms in the pyrochlore structure, as well as to elucidate short- *vs.* long-range structural properties [6-9]. In this context, there is a long-standing discussion in the literature as to whether the order-disorder processes are driven by anions, cations or by both simultaneously [10-13]. Despite the substantial amount of experimental work completed by the scientific community, a complete understanding of the fundamental aspects controlling defect´s formation and annihilation remains elusive.[14-18] The present contribution addresses this issue by analyzing the effect of doping and processing conditions on the structural and microstructural features of bulk gadolinium zirconate powders, $Gd_2Zr_2O_7$ (GZO). These results are discussed in the context of the existing criteria for predicting the formation and stability of pyrochlore oxides of different compositions.

Ideal (ordered) pyrochlore oxides are isometric [S.G. = $Fd\bar{3}m$ (227), Z = 8] and characterized by the $A_2B_2O_6O'$ ideal stoichiometry, where A, and B are cations and O and O' represent two nonequivalent oxygens[19]. Selecting the second choice of origin for the space group, O and O' fully occupy the 48f (x, ⅛, ⅛), and 8b (⅜,⅜,⅜) Wyckoff sites, respectively. Although both are tetrahedrally coordinated, each O ion (O_{48f}) has two A and two B nearest neighbors, and each O' (O_{8b}) is surrounded by four A metal atoms. The B cation (r_B ~ 0.6-0.7 Å) sits at the center of a trigonal antiprism, with six equidistant O_{48f} ions (Wyckoff 16c site (0,0,0)). The A cation (r_A ~0.9-1.2 Å) sits at the 16d position (½,½,½), surrounded by eight anions forming an axially compressed scalenohedron: *i.e.*, two metal-oxygen bonds <A-O_{8b}> are significantly shorter than the remaining six, <A-O_{48f}>. Noteworthy is the existence of an additional interstitial site in the unit cell,

Wyckoff site 8a (⅛,⅛,⅛), which is nominally vacant in the ideal pyrochlore structure, but easily accessible for anions in defect phases. As with the 48f, and 8b positions, the 8a-site is also tetrahedrally coordinated, though by four B cations. This vacant site provides the pyrochlore structure with the remarkable ability to tolerate structural distortions. Moreover, pyrochlore oxides can accommodate variable degrees of cation and/or anion disordering depending on intrinsic (*e.g.*, chemical composition, bonding character and cations size mismatch, r_A/r_B) as well as extrinsic factors (*e.g.*, thermal history and processing conditions). Thus, radius ratio constraints based on the cations for lanthanide zirconates, $Ln_2Zr_2O_6O$', result in pyrochlore formation only when $r_{Ln}/r_{Zr} \geq 1.46$[19]; whereas, the size mismatch favors a change to anion deficient fluorite structures below 1.46 (Ln = Tb-Lu and Y). Figure 1 shows schematic representation of the structures of fluorite, ideal pyrochlore and disordered pyrochlore. Gadolinium zirconate, $Gd_2Zr_2O_7$ (GZO), is probably the most thoroughly studied member of the series; in addition to high thermal and chemical stability, GZO shows high oxygen ion mobility at elevated temperatures ($\sigma > 10^{-3}$ S·cm^{-1} at 800ºC [20, 21]), and very low thermal conductivity ($\kappa \sim 1.5$-2 W·m^{-1}·K^{-1} [22, 23]). Therefore, GZO is considered a promising electrolyte candidate material for solid oxide fuel cells, as well as a suitable ceramic coating to provide thermal insulation to the metal components of gas turbines and diesel engines. Furthermore, GZO shows great potential to incorporate actinides in solid solution and is highly tolerant to radiation damage [24, 25]; hence, GZO is under consideration as a host phase for the chemical immobilization of plutonium from dismantled nuclear weapons.

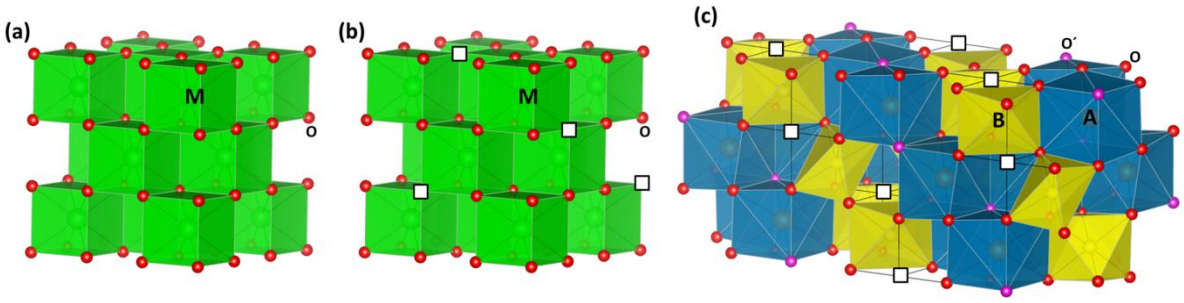

Figure 1. Schematic representation of the structures of: (a) ideal stoichiometric fluorite with composition MO_2 where only one site for metal ions and anions exist being both substructures fully occupied with random distribution of metal ion in mixed fluorite. (b) anion-deficient fluorite (or disordered defective pyrochlore) in which only one site for metal ions and oxygen exist, anion vacancies (denoted as □) are randomly distributed in the structure. (c) ideal pyrochlore structure $A_2B_2O_7$ with two sites for metal ions (A and B) and two sites for oxide anions; A and B are ordered as well as oxygen vacancies which are located in the B-cation coordination sphere resulting in $BO_6\square_2$ trigonal antiprisms in contrast to AO_8 cubes or scalenohedra.

This paper analyzes the effect of intrinsic (cation size mismatch), and extrinsic (processing) factors, in the degree of structural order/disorder of bulk GZO. GZO was selected for this study because it lies precisely, at the boundary between the pyrochlore and fluorite stability fields (r_{Gd}/r_{Zr} = 1.462). In fact, GZO presents a thermally-induced solid state phase transition to a disordered anion deficient fluorite-like structure, at ~1550ºC. Therefore, small changes in the cation size ratio alter the relative stability of both structures. Accordingly, six substituting cations were selected amongst lanthanide ions larger (Nd^{3+} and Sm^{3+}) and smaller (Dy^{3+}, Ho^{3+}, Y^{3+}, and Er^{3+}) than Gd^{3+}. Furthermore, two different levels of substitution were chosen for each cation to

cover a wide range of r_A/r_B values. All samples were prepared by mechanical milling; mechano-chemical powder processing methods (dry or liquid-assisted) have become very popular in all areas of materials science [26-29] because they are cost-effective and rather simple to implement. As a far-from-equilibrium technique, mechano-chemical methods frequently lead to uncommon and highly defective phases, which are inaccessible for more conventional processing methods. More attractive even for the purposes of this study, is the possibility of unlocking multiple metastable intermediate states *via* additional processing (*e.g.*, annealing), with controlled defect structures and functionalities.

EXPERIMENTAL

Samples with the general formulae $Gd_{2-x}Ln_xZr_2O_7$ (Ln = Nd^{3+}, Sm^{3+}, Dy^{3+}, Ho^{3+}, Y^{3+}, and Er^{3+}; x = 0.20 and 0.80) were prepared by milling stoichiometric mixtures of high-purity Ln_2O_3, and ZrO_2 oxides (≥ 99.9%, Sigma-Aldrich, Inc.), as described in previous works completed by some of the present authors [21, 23]. Powders were weighed out according to the desired stoichiometry and placed in 125 ml YPSZ (yttria partially stabilized zirconia, 5wt% Y_2O_3) containers together with six 20 mm diameter YPSZ balls as grinding media (mass ~25 g; balls-to-powder mass ratio equal to 10:1). Most lanthanide sesquioxides are highly reactive towards atmospheric H_2O, and CO_2. Therefore, starting Ln_2O_3 chemicals were fired overnight at 900°C, to decompose existing hydroxides, carbonates, and/or oxycarbonates and to ensure retention of the designed stoichiometries. In a typical experiment, a 15 g batch of reactants were dry milled in a planetary ball mill using a rotating disc speed of 350 rpm, with a reversed rotation every 20 minutes, to favor reaction. The evolution of the starting mixtures with milling time, was followed by

characterization using X-ray powder diffraction (Philips X'Pert diffractometer, and Ni-filtered Cu-Kα radiation, λ = 1.5418 Å). Milling time needed to achieve single phase products was determined by examination at different time intervals of the X-ray diffraction patterns of two samples selected as representatives of the series; these two samples were $Gd_{1.2}Nd_{0.8}Zr_2O_7$, and $Gd_{1.2}Er_{0.8}Zr_2O_7$ which represent the highest substitution level attempted in this work (0.8), and the largest Ln^{3+} size difference with the Gd^{3+} host. Moreover, mechanically-induced chemical reactions were considered completed after 30 hours, when no traces of the starting reagents were evident in the x-ray diffraction patters. To minimize any possible processing effect on the final structural/microstructural characteristics of the as-prepared powders, the same milling parameters were used to prepare every sample analyzed in this work. To examine the annihilation of mechanically-induced defects as a function of temperature and chemical composition, as-obtained powder samples were fired 12 h at 800 ºC and 1400ºC and characterized as explained below.

The structural and microstructural features of every sample were obtained from precise diffraction data collected using conventional and synchrotron X-ray sources. Laboratory X-ray diffraction data were collected on a Bruker D8 high-resolution instrument equipped with a Ge primary monochromator (CuKα1 radiation, λ = 1.5406 Å), and a Position Sensitive Detector (PSD) MBraun PSD-50M. Data collection parameters (measured angular range, step size, and counting times) were selected to ensure enough resolution (the step size should be at least, 1/10 of the FWHMs) and good statistics for the diffraction analysis. The instrumental contribution to line broadening was evaluated using NIST LaB_6 standard reference material (SRM 660a; μ = 1138 cm^{-1}, linear absorption coefficient for CuKα1 radiation). Synchrotron X-ray data (SXRD) were collected at room temperature at beamline 16-ID-B of HPCAT, Advanced Photon Source at Argonne National Laboratory, in transmission mode, using a monochromatic X-ray beam with a

wavelength of 0.4066 Å. The Debye rings were recorded with a CCD detector and integrated into two dimensional patterns using the FIT2D software [30]. The instrumental contribution to the synchrotron XRD pattern was calibrated by using high purity CeO_2 powder as standard. Structure refinements were completed by the Rietveld method using the FullProf software package [31], simultaneously taking into account the effect of each sample's microstructure on the diffraction patterns, according to a phenomenological approach described in detail elsewhere [32-35]. Samples were also characterized by Raman spectroscopy using a Bruker FT-Raman RFS 100/spectrometer. Excitation was achieved by using a YAG:Nd^{3+} laser (1064 nm) and the spectral resolution was 2 cm^{-1}. To avoid luminescence, different laser lines were used for Er, Nd (Horiba-Yvon, 488 nm), and Ho containing samples (Renishaw, 830 nm).

RESULTS

Defects and disorder in the pyrochlore structure

The pyrochlore structure is commonly depicted as an ordered derivative of the anion-deficient fluorite structure (Figure 1); accordingly, the XRD pattern of an ideal pyrochlore oxide contains a set of strong diffraction maxima characteristic of the underlying fluorite-type subcell, plus an additional set of weak superstructure diffraction lines [10]. The intensity of the superstructure peaks depends on factors such as the degree of atomic ordering, the chemical composition (differences in the average scattering factors), and the distribution of oxygen vacancies. As mentioned above, the extent of disorder in GZO is particularly sensitive to doping, and/or processing conditions. Therefore, replacing Gd^{3+} by different lanthanides, Ln^{3+}, modifies the nominal r_A/r_{Zr} ratio and the relative stability of the pyrochlore and fluorite structures (see Table 1).

Table 1. Effect of substituting Ln^{3+} ions in the cation size mismatch of $Gd_{2-x}Ln_xZr_2O_7$

Substituting ion	***Ionic radius***	***Averaged r_A***		***r_A/r_{Zr} ($Gd_{2-x}Ln_xZr_2O_7$)***	
		***x* = 0.20**	***x* = 0.80**	***x* = 0.20**	***x* = 0.80**
Nd^{3+}	1.109	1.059	1.075	1.490	1.493
Sm^{3+}	1.079	1.056	1.063	1.466	1.477
Gd^{3+}	**1.053**	**1.053**	**1.053**	**1.462**	**1.462**
Dy^{3+}	1.027	1.050	1.043	1.459	1.448
Y^{3+}	1.019	1.050	1.039	1.458	1.444
Ho^{3+}	1.015	1.049	1.038	1.458	1.441
Er^{3+}	1.004	1.048	1.033	1.456	1.439

$$\text{Averaged } r_A = \frac{(2-x)\, r_{Gd} + x\, r_{Ln}}{2};\ (r_{Zr} = 0.72\ \text{Å})$$

Ionic radii values used to build Table 1, are those given in [36].

Structural characterization

Samples just-milled, and milled/fired at 800°C

Irrespective of the substituting ion and according to XRD data obtained using a conventional X-ray source, both series of samples (just-milled, and milled/fired at 800°C) form a fluorite-like structure. To illustrate this point, Figure 2 shows two representative XRD patterns belonging to the sample featuring the largest dopant-to-host size difference of the series, $Gd_{1.20}Nd_{0.80}Zr_2O_7$. Broad diffraction lines as those observed in Figures 2a and 2b, are usually characteristic of highly stressed mechano-chemically prepared powders, with a small crystalline domain size. The only apparent difference between both XRD patterns is the width of the diffraction peaks which, as expected, are narrower in the annealed samples.

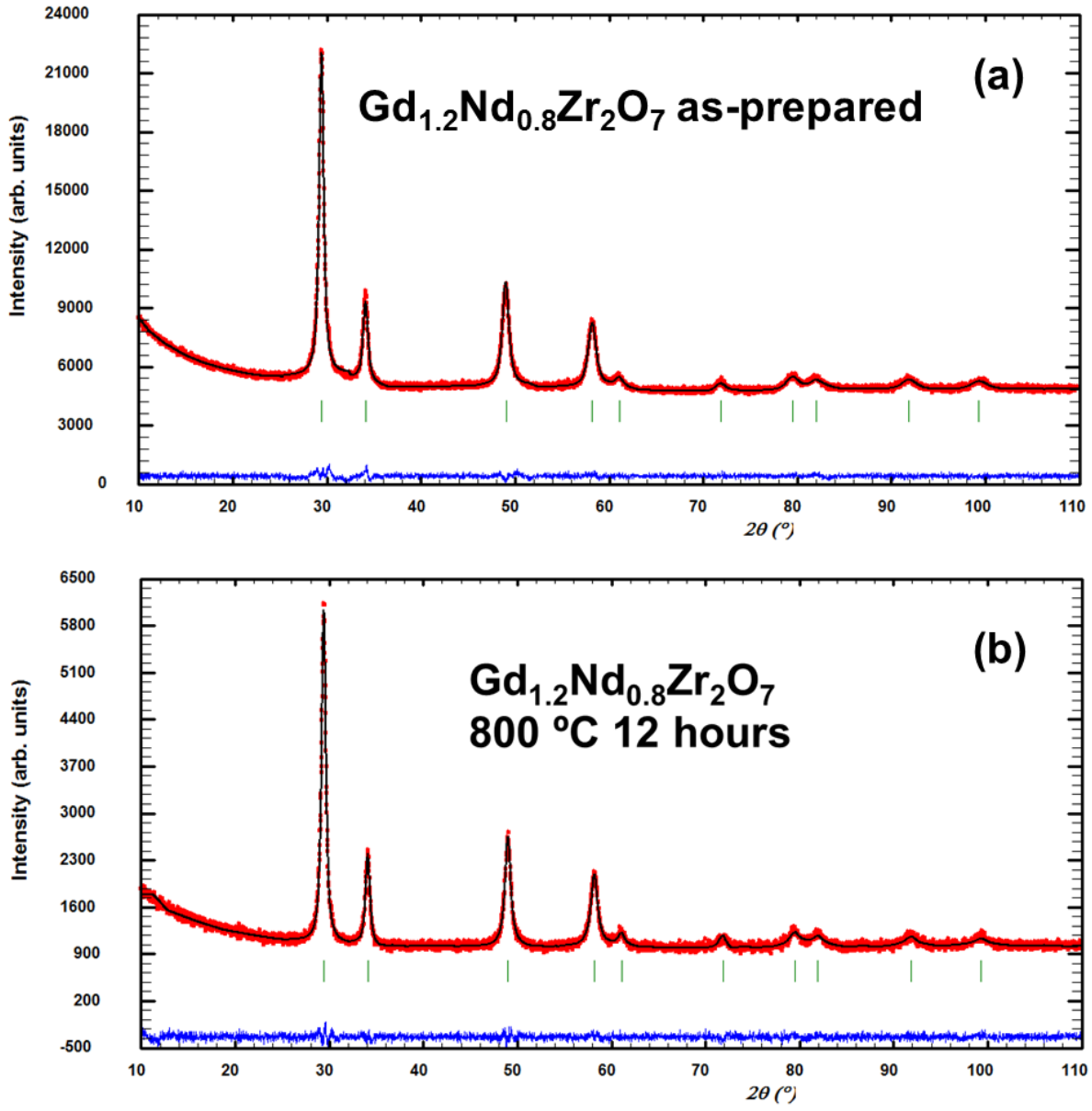

Figure 2. Experimental (red circles) and calculated (black solid line) XRD patterns and their difference (bottom blue line) of the as-prepared $Gd_{1.20}Nd_{0.80}Zr_2O_7$ sample (a), and (b) after annealing at 800°C.

Unit cell parameters of as-prepared and annealed at 800ºC series, given in Table SI 1, are plotted in Figure 3, as a function of the averaged A-site cation size. In general, the cell parameter, which

is the only free parameter in the fluorite structure, increases with the averaged A-site cation size, except for the $Gd_{1.20}Nd_{0.80}Zr_2O_7$ sample. As shown in Table 1, this composition features the largest dopant-to-host size mismatch (highest r_A/r_B ratio) of the whole series and in consequence, would have the strongest driving force for pyrochlore ordering. Although Figures 2a and 2b do not show any evidence of superstructure peaks, the anomalously short unit cell determined from the XRD data could be a signature of short range ordering: *i.e.,* Gd^{3+}/Nd^{3+} and Zr^{4+} may be ordered within a given unit cell but this order is lost in neighboring cells, limiting ordering in this sample to the very short-range.

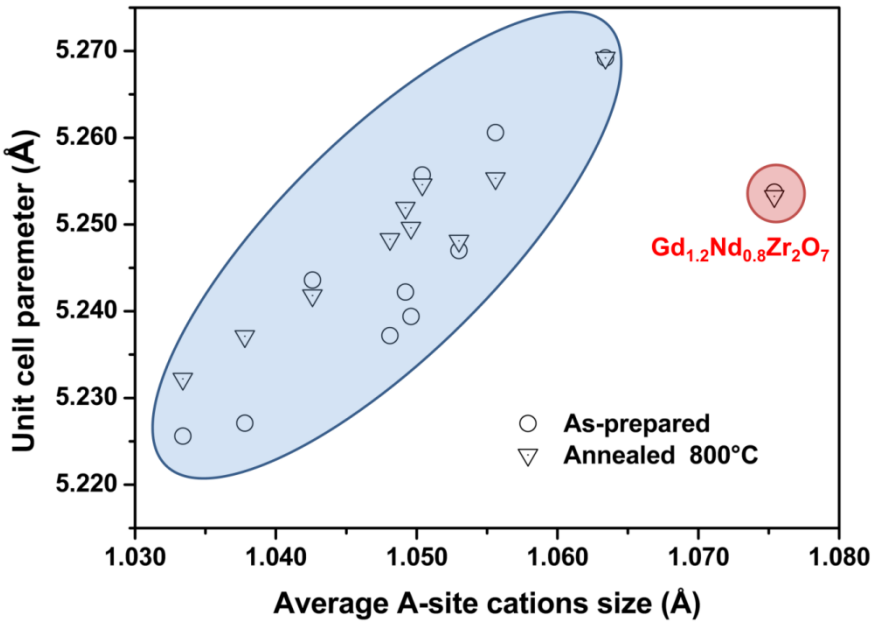

Figure 3. Evolution of the unit cell length with the averaged *A*-site cations size: just-milled powders (empty circles), and the same samples after annealing at 800ºC (empty triangles).

As for the remaining samples, the unit cell expands in most cases on firing at 800ºC. Since the cell parameter in $(A,B)O_{1.75}$ fluorite structures is related to the metal-metal distance <A-B>, such

increment might be correlated with the relaxation of internal stresses; *i.e.*, this temperature is not sufficiently high to promote an extensive structural rearrangement to induce a phase transition to the pyrochlore structure (disorder-order transformation), but it is high enough to allow some microstructural relaxation. Moreover, the samples microstructural features (size and strain-induced line-broadening) were obtained from the corresponding Langford plots[32, 33, 35]. As an example, Figures 4a and 4b present such plots for the $Gd_{1.80}Dy_{0.20}Zr_2O_7$ sample, just-milled, and fired at 800°C, respectively. On its hand, Figures 4c and 4d show the domain size and strain in both series of fluorite-like materials plotted as a function of an averaged A-site cation size, respectively.

As shown in Figure 4c, the domain size does not change very much with the A-site cation size and remains similar within each series of samples; apparently, the only effect of annealing at 800°C is a relatively modest crystallite growth from ca. 100 Å to ca. 120 Å diameters. By contrast, the strain seems to be slightly positively correlated with the A-site cation size (and consequently with the r_A/r_B ratio), which might be an indication of an increasing tendency to metal ordering as the A-to-B cation size mismatch increases. Although some relaxation seems to occur after a soft thermal treatment at 800°C, all samples fired at this temperature remain highly stressed.

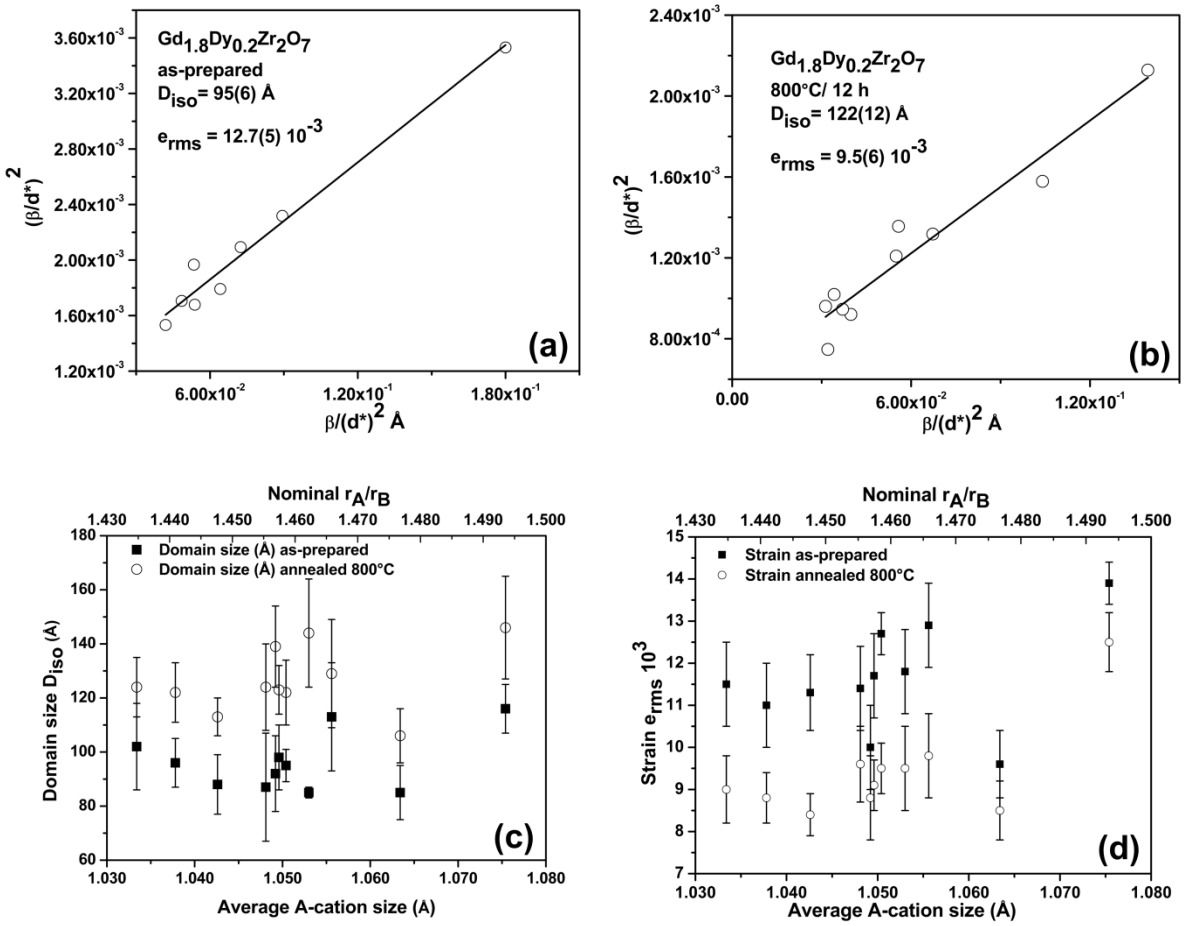

Figure 4. Langford plots obtained for the as-prepared $Gd_{1.80}Dy_{0.20}Zr_2O_7$ powders (a) and the same sample after firing 12 h at 800°C (b); domain size (c), and strain (d) plotted as a function of the averaged *A*-site cation size for both series of samples, just-milled (solid squares) and milled and fired at 800°C (empty circles).

Samples milled and fired at 1400°C

For samples milled and treated at high temperature (1400°C for 12 hours), the result is more complex but far more interesting. Therefore, to get a better understanding of the structural/microstructural characteristics of these mechano-chemically obtained and high-

temperature annealed oxides, conventional and synchrotron XRD data were combined as explained in the Experimental section. Figure 5a shows the graphic result of fitting XRD data obtained using a conventional X-ray source corresponding to the $Gd_{1.20}Nd_{0.80}Zr_2O_7$ sample; whereas Figure 5b displays a similar plot for $Gd_{1.80}Y_{0.20}Zr_2O_7$, but obtained using synchrotron data (SXRD). As shown for the example in Figure 5a, some annealed sample compositions display all of the pyrochlore superstructure peaks. However, the only superstructure diffraction maximum observed in some others, such as that shown in Figure 5b, is the very weak (111) peak with $(½\ ½\ ½)_F$ Miller indexes in the basic fluorite cell. The complete refined structural parameters for the entire series are given in Table SI 2.

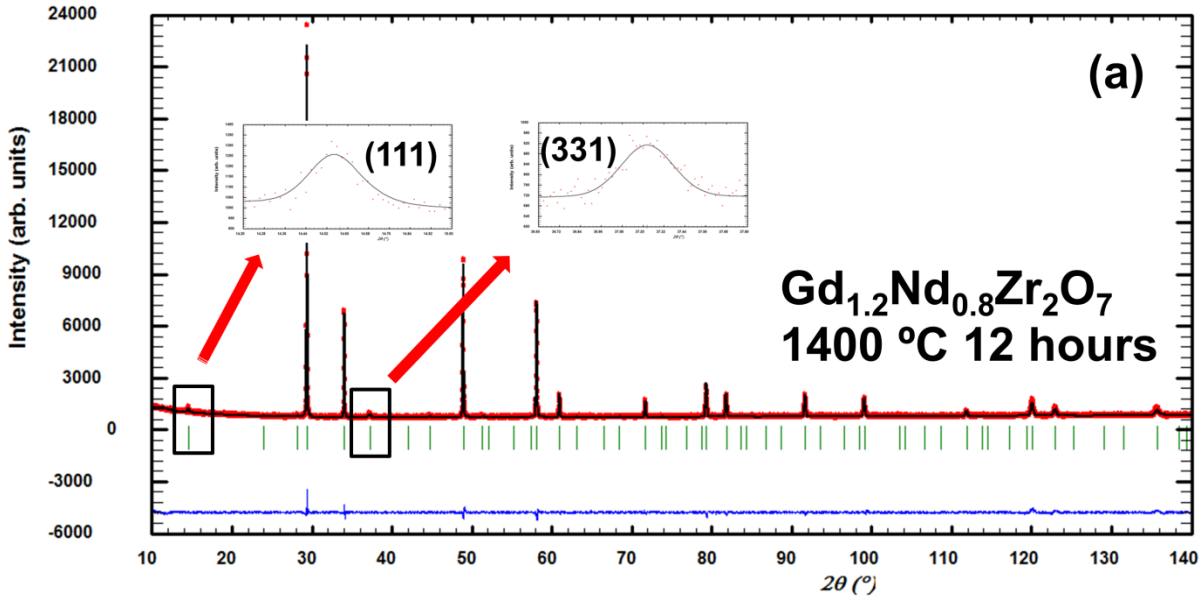

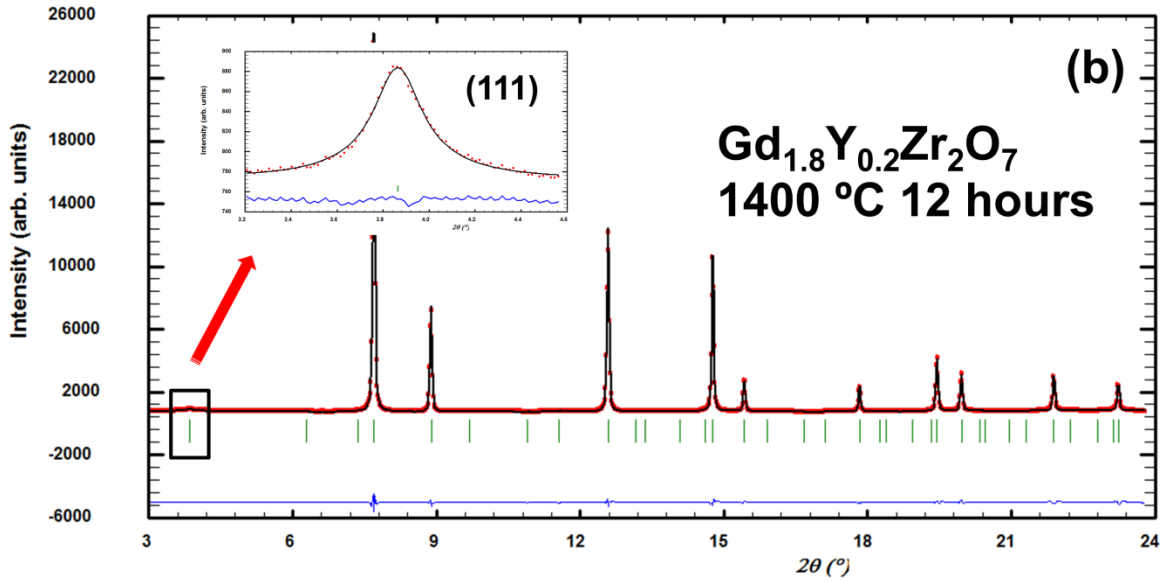

Figure 5. Graphic result (experimental, calculated and their difference as labelled in Figure 2) of the fitting of (a) laboratory XRD data for the $Gd_{1.20}Nd_{0.80}Zr_2O_7$ sample and (b) synchrotron XRD data for $Gd_{1.80}Y_{0.20}Zr_2O_7$, both obtained by milling and fired 12 h at 1400°C. Insets in both figures enlarge some pyrochlore superstructure peaks.

Two key points should be stressed:

1) Very often, the distribution of metal ions in our samples is not that expected for an "ideal" ordered pyrochlore structure*, i.e.,* even after firing at such a high temperature, varying degrees of disorder are observed in the series, with some Zr^{4+} ions occupying the 8-fold A-site and correspondingly, some Gd^{3+}/Ln^{3+} ions sitting at the 6-fold B-site.

2) The domain size of the ordered pyrochlore regions in some samples is very small.

These two features make it rather difficult to predict the structure of any specific sample based only on its chemical composition (this will be discussed in detail), as well as to refine the diffraction data. To overcome these drawbacks, the degree of inversion (*i.e.,* the proportion of Gd^{3+} ions in the B-site) obtained from the Rietveld refinement, was confirmed by correlating this parameter (calculated), with the ratio between the experimental integrated intensities of the (111) and (222) superstructure Bragg maxima, the $I_{(111)}/I_{(222)}$ intensity ratio. The first maximum depends on the distribution of cations between the A- and B-sites; whereas, $I_{(222)}$ depends only on the total scattering power in A- plus B-sites. Since the number of superstructure peaks observed is limited in most cases, even high-intensity SXRD data did not allow us to use the Langford plots to determine the pyrochlore domain size, as previously done for the samples treated at 800 C. In any case, domains seem to be fairly small because, as shown in Figure 6, the superstructure maxima are, in general, very broad. Furthermore, the (111)-peak is absent for some samples (*i.e.,* substituting ions smaller than Gd^{3+} and largest substitutional level) (Fig. 6), with $Gd_{1.80}Y_{0.20}Zr_2O_7$ being the last sample in the series showing superstructure maxima due to pyrochlore-type ordering.

Interestingly, in all the samples treated at high temperature the size of the fluorite sub-structure domains is pretty large regardless the composition and, consequently, the actual r_A/r_B ratio. The fluorite domain size can roughly be estimated to be greater than 2000Å, being this a widely accepted limit to applied those methods to estimate crystallite size from diffraction peaks broadening. [34, 35] As shown in Figure SI 1 for the two extreme values of r_A/r_B on Table 1, only subtle peak broadening is observed due to domain size effects when compared with NIST standard LaB_6.

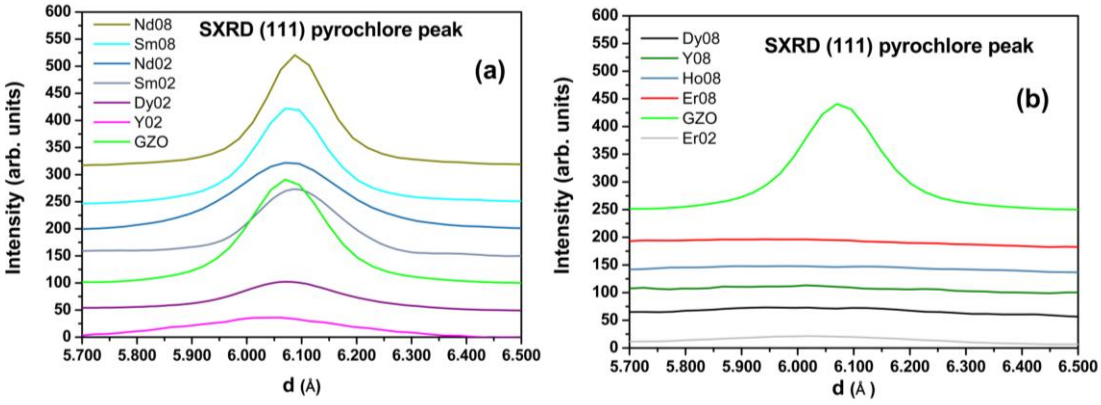

Figure 6. Enlargement of the SXRD patterns of the $Gd_{2-x}Ln_xZr_2O_7$ series at the position of the (111) superstructure peak characteristic of pyrochlore ordering. In panel (a) are shown those materials with pyrochlore structure, in (b) those without long-range ordering. $Gd_2Zr_2O_7$ is depicted in both panels for comparison.

Raman spectroscopy

As structural disorder within the pyrochlore structure loses its translational symmetry, Raman spectroscopy can be used to investigate the nearest-neighbor changes in the structure. Note, disordering allows more phonons to contribute to the optical spectra, thus causing a general broadening of all Raman active modes. Furthermore, according to the selection rules, the $(A_{0.5}B_{0.5})O_{1.75}$ anion deficient fluorite structure should have only one Raman-active mode of F_{2g} symmetry, with the form of oxygen anions vibrating against the symmetry-fixed cations [37]. By contrast, $A_2B_2O_7$ pyrochlore-type phases should have six Raman-active modes [38]. Five of them

(*i.e.,* $A_{1g}+E_g+3F_{2g}$), are commonly assigned to vibrations of O_{48f} ions and the remaining one (F_{2g}), to vibrations of the O_{8b} ions. Specifically, only O_{48f} ions vibrate in A_1 and E_g modes (predominantly bending vibrations); furthermore, A_{1g} is directly related to the only free positional parameter of the pyrochlore crystal structure, the x_{48f} parameter. Moreover, an eventual pyrochlore-to-fluorite phase transition or even higher structural disorder without a phase transformation should lead to significant broadening and/or to a drastic reduction in the number of modes observed by Raman spectroscopy. However, short-range ordering of cations and oxygen vacancies is almost invariably present in any fluorite sample obtained by disordering the pyrochlore structure. In fact, recent work has shown that the local atomic arrangement of this disordered, defect-fluorite structure, is more ordered than previously thought and can be best modeled by the fluorite-derivative weberite-type (Ccmm) structure [9]. The same type of short-range order was even found in amorphous pyrochlore compositions and seems to be a universal phenomenon in non-ordered phases.[39, 40] Accordingly, the Raman spectra of fully-disordered pyrochlore samples show, usually, more bands than expected for a truly ideal anion deficient fluorite structure [37, 38, 41-43]. Figure 7 compares the Raman spectra of pristine GZO (just-milled (JM), fired at 800 and at 1400°C) and those obtained for the cation substituted samples, after firing them at 800 (Figure 7a) and 1400°C (Figure 7b). As shown in Figure 7a, structural disorder in the just-milled GZO (GZO JM), reduces its Raman spectrum to a broad, almost featureless density-of-states continuum, with no well-defined absorption bands. The Raman spectrum of GZO does not change much on firing at 800°C, although very broad Raman active bands start to appear at ~331, ~381, ~560 and ~625 cm^{-1}. Both spectra are very similar to those obtained in this study for $Gd_2(Ti_{0.65}Zr_{0.35})_2O_7$ just-milled and annealed at 600ºC, which had fluorite-type structures [37, 38, 41-43]. The only difference is the lack of a broad and relatively intense

band at 750 cm^{-1}, which has been attributed in the literature to disorder-activated oxygen vibrations [41].

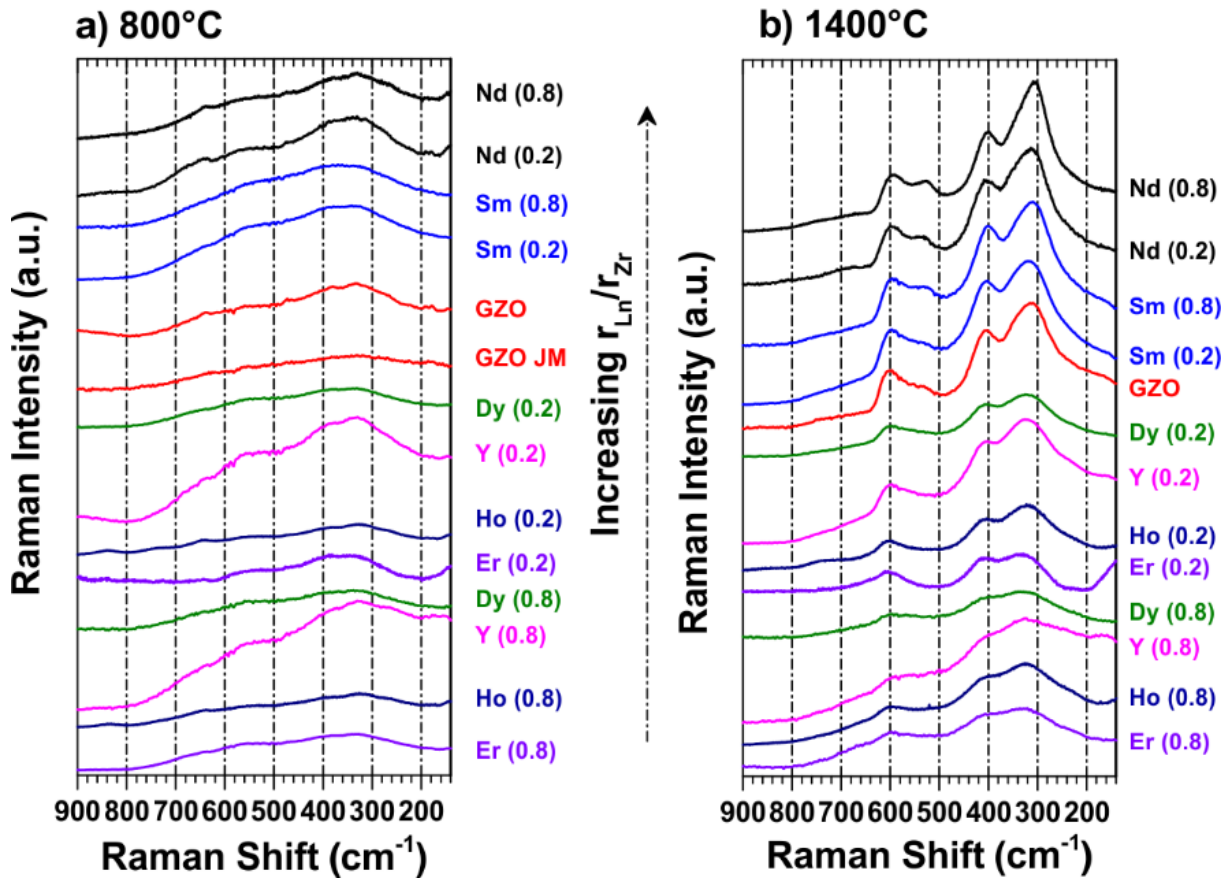

Figure 7. Raman spectra for samples fired at 800 (a) and 1400°C (b). Each sample is identified by specifying the chemical symbol of the substituting lanthanide and the level of substitution in parenthesis. GZO stands for $Gd_2Zr_2O_7$ and JM for "just-milled".

Therefore, Raman spectroscopy confirms that just-milled GZO has a fluorite-type structure and that it is stable even after firing at 800°C. The intensity of the observed Raman bands increases, and at the same time, their width decreases as the annealing temperature increases to 1400 °C (spectrum in red color in Figure 7b); the most intense band in this spectrum is observed at ~314 cm^{-1}. Additional bands are observed at ~405, ~537 and ~600 cm^{-1}. A similar spectrum was obtained for a $Gd_2Zr_2O_7$ ceramic prepared by solid-state reaction at 1430°C [44]. Furthermore, a very broad and weak band appears at ~740 cm^{-1}. All these features corroborate the formation of a pyrochlore-type structure on firing although the presence of the band at ~740 cm^{-1} and the large bandwidth of all other peaks are indicative of residual oxygen disorder. As for the samples with substituted lanthanides, irrespective of the lanthanide ion involved and the level of substitution, the Raman spectra obtained after firing at 800°C all are similar and suggest the formation of fluorite-type structures, in agreement with the XRD analysis. The Raman spectra obtained for the $Gd_{1.20}Nd_{0.80}Zr_2O_7$ sample, do not support the existence of short-range pyrochlore-like ordering, which might have explained the anomalous short unit cell parameter determined from the XRD data.

Clear differences between substituting lanthanide ions arise when the samples are treated at 1400°C. Therefore, the Raman spectra obtained for all cations smaller than Gd^{3+} suggest the formation of a pyrochlore-type structure when x = 0.20. Pyrochlore-like phases seem to be also formed for Ho^{3+}, Dy^{3+} and Er^{3+}, when the level of substitution increases to x = 0.80; however, broader bands as compared with the samples where x = 0.20, suggest a higher degree of structural disorder. Yttrium deserves special mention since even after firing at 1400°C, the Raman spectrum of the $Gd_{1.20}Y_{0.80}Zr_2O_7$ sample, lacks well-defined bands and looks more like that of a fluorite phase. Having almost the same ionic radii and electronegativity of Ho^{3+}, yttrium

induces a higher degree of oxygen disorder in GZO. As for the lanthanide ions larger than Gd^{3+}, both Sm^{3+} and Nd^{3+} produce Raman spectra characteristic of better ordered pyrochlore structures. However, increasing Sm^{3+} content does not seem to have much effect on ordering; whereas, increasing Nd^{3+} incorporation produces more order than Sm^{3+} as evidenced by the well-developed band at 525 cm^{-1}.

In summary, according to XRD and Raman spectroscopy, all as-prepared samples seem to crystallize in fluorite-like structures, which are stable even after firing at 800ºC. Some discrepancies arise apparently between these two techniques, when analyzing the samples fired at 1400°C. Moreover, both techniques suggest pyrochlore-like ordering for pristine and lanthanide-substituted GZO, when the lanthanide ion is larger than Gd^{3+}. However, when the lanthanide ion is smaller than Gd^{3+}, according to Raman spectroscopy, only $Gd_{1.20}Y_{0.80}Zr_2O_7$ maintains the fluorite structure after firing at 1400°C. The remaining lanthanide-substituted materials are pyrochlore-like phases but featuring a different degree of structural disorder depending upon the lanthanide ion involved and the amount of lanthanide substitution. In contrast, XRD (conventional and synchrotron) suggest a fluorite-type structure when x = 0.80, for all lanthanide ions smaller than Gd^{3+}, and for both Er-containing samples (x = 0.20 and 0.80). These discrepancies can be explained by recalling that spectroscopic techniques provide information on local order, *i.e.,* they can reveal short-range features (such as the superstructure ordering resulting in the pyrochlore structure); whereas, diffraction techniques can only detect structural effects extending at least for some hundreds of angstroms. Therefore, in those cases where the superstructure maxima are not observed even by SXRD, it might be due to a very local ordering that can be detected by Raman but not by X-ray diffraction methods. In this context,

Figure 8 shows the evolution of the pyrochlore-domain size along the series as estimated by the Scherrer formula from the width of the (111)-peak.

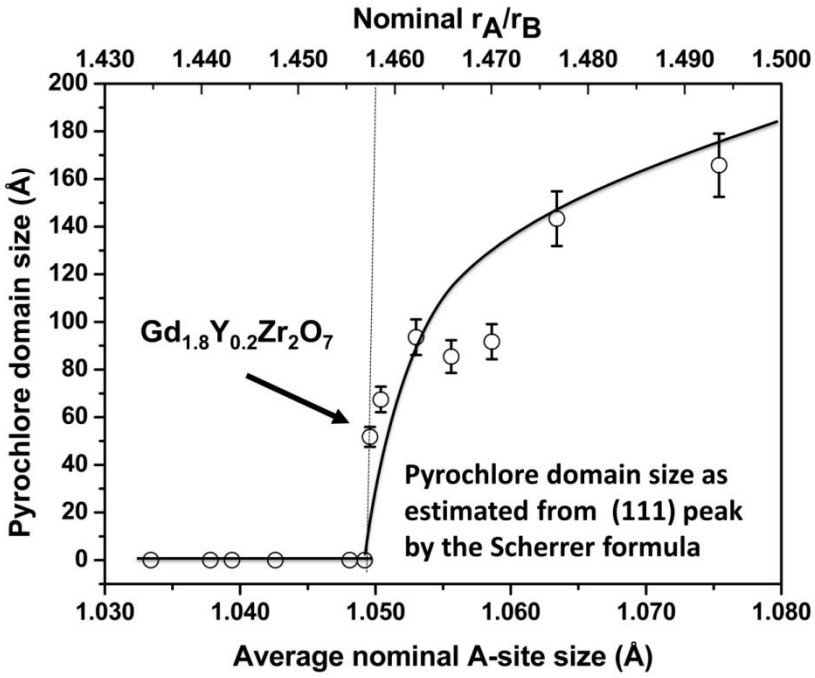

Figure 8. Pyrochlore-like domain size as estimated by Scherrer's formula using the (111) diffraction peak for samples annealed at 1400ºC. The continuous line is a guide for the eye.

Although the Scherrer approach underestimates the domain size [45], a clear trend is observed in Figure 8. The size of the ordered pyrochlore domains decreases as the averaged A-ion radius decreases, suggesting a lower tendency to order; for ion size below 1.050 Å (corresponding to a r_A/r_B size ratio of 1.457), no ordering effects are detected by SXRD. As Raman spectra suggest, this is due to a reduction of the ordering distance below the coherence length of diffraction

techniques. Finally, the compound $Gd_{1.20}Y_{0.80}Zr_2O_7$ seems to be somewhat special since neither diffraction nor spectroscopic measurements detected any degree of order.

DISCUSSION

The use of a simple parameter such as the Goldschmidt tolerance factor, t, is of great help in understanding, and even predicting, structural and physical properties of perovskite-like materials. Therefore, defining a similar tolerance factor for pyrochlore-like compounds would be of noticeable importance. Several approaches based on chemical composition, have been used in the literature to predict whether a hypothetical compound will crystallize in a pyrochlore-type structure when allowed to reach the thermodynamic equilibrium at sufficiently high temperature (1400º C in the present case). As mentioned before and it is illustrated in Figure 9, the simplest criterion would be the radius ratio rule, *i.e.,* a pyrochlore structure will form when $r_A/r_B \geq 1.46$; whereas, the fluorite structure would be more stable, when $r_A/r_B < 1.46$ (red and green shaded boxes respectively).[19] Also depicted in Figure 9 is the evolution of the r_A/r_B ratio in the $Gd_{2-x}Ln_xZr_2O_7$ series as a function of the nominal (averaged) A-cation size (empty squares), *i.e.,* that determined for each sample assuming cations distribution based on ionic size and crystallochemical criteria. Interestingly, when the r_A/r_B size ratio is calculated using the actual occupancies of both sites *(i.e.,* that obtained from the XRD data using the Rietveld method), the pyrochlore stability field expands slightly towards lower r_A/r_B values (filled circles), with the boundary lying now at $r_A/r_B \approx 1.457$. Also plotted in the same Figure is the degree of inversion (empty circles), given as the percentage of the A-site occupied by B-ions (or *vice versa*), as obtained from the Rietveld refinement (Table SI 2). Figure 9 suggests the existence of a

correlation between the pyrochlore-to-fluorite phase transition and the degree of inversion: as the latter tends to 50% (fully disordered fluorite), the nominal r_A/r_B ratio approaches the limiting value and, more interestingly (and more meaningful), the actual r_A/r_B ratio tends to unity (as corresponds to A- and B-sites equally populated by Ln^{3+}, and Gd^{3+} ions). Even for the samples consisting of large ordered pyrochlore-domains such as $Gd_{1.20}Nd_{0.80}Zr_2O_7$, some degree of inversion exists, *ca.* 10%. This can be due to the mechano-chemical synthesis procedure used since it might be possible that a treatment at 1400ºC for 12 hours is not sufficient to reach the atomic configuration corresponding to the thermodynamic equilibrium; consequently, some mechanically-induced defects remain in our high-temperature annealed samples.

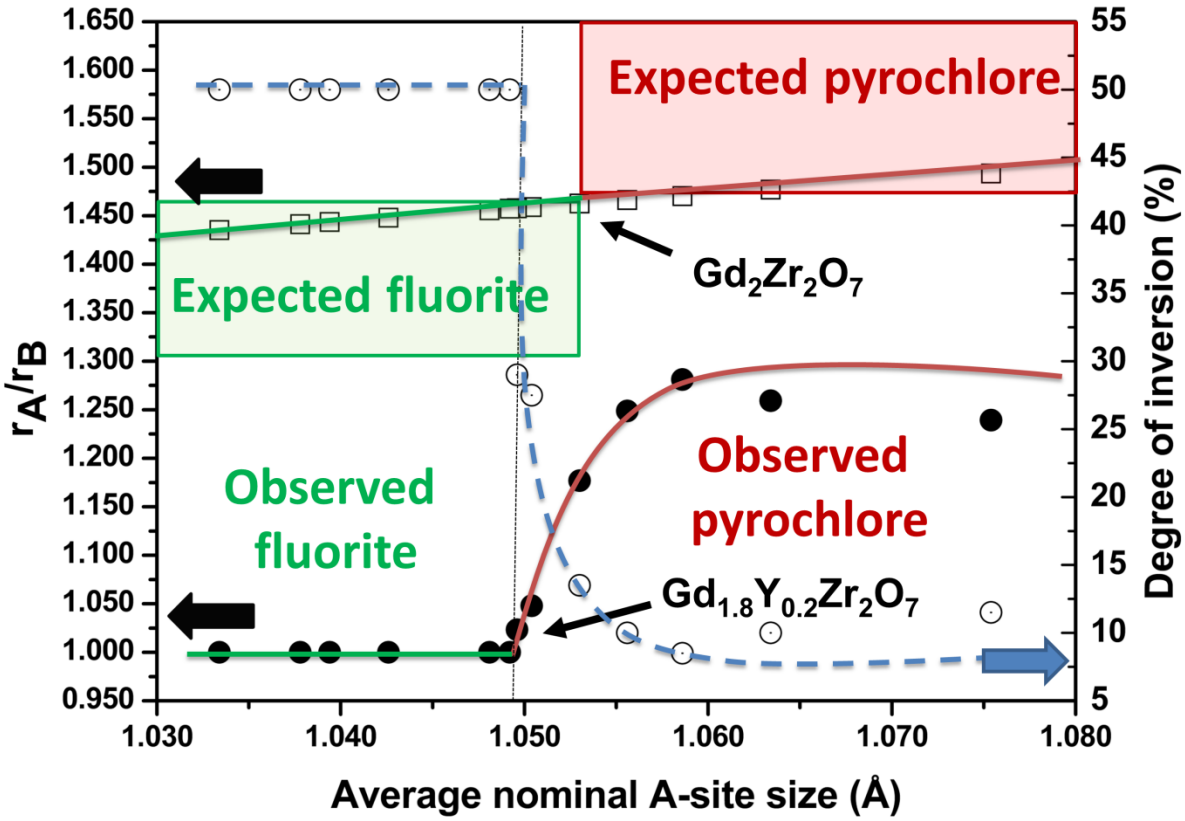

Figure 9. Size ratio (r_A/r_B) and degree of inversion (empty circles) in $Gd_{2-x}Ln_xZr_2O_7$, plotted as a function of the averaged A-cation size. Empty squares represent the nominal r_A/r_B values obtained using the theoretical cations distribution of each composition; whereas, filled circles represent experimental r_A/r_B values, which were calculated using the cation distribution obtained by the Rietveld method. Lines are guides for the eye.

The first attempt to propose a tolerance factor for pyrochlore oxides like that used for perovskites, was that of Isupov according to Eq. [1]:

$$t_I = 0.866\ [(r_A + r_O) / (r_B + r_O)] \qquad [1]$$

where r_A, r_B and r_O are the size of the A, B and oxygen ions, respectively [46]. In this expression the value 0.866 is the distances ratio $d(A\text{-}O_{48f})/d(A\text{-}O_{8a})$ when BO_6 is a perfect octahedron. However, as pointed out by Subramanian, [19] this assumption is hardly achieved in pyrochlore oxides resulting to incoherent and meaningless t_I values. As Figure 10 shows (empty squares), for our high-temperature annealed samples, a smooth variation of t_I within a very narrow range (from 1.015 to 0.995), is observed along the $Gd_{2-x}Ln_xZr_2O_7$ series when using the nominal composition, *i.e.*, if all Zr^{4+} ions were located at the six-fold coordinated sites and all Ln^{3+} ions in the 8-fold A-sites. By contrast, the pyrochlore-to-fluorite transition is clearly associated with a t_I value of 0.866 when using the experimental ion distribution obtained by the Rietveld method (full circles). In any case, this parameter seems to have little practical utility because the

structure of any particular compound should be known beforehand; therefore, it does not represent any advantage in comparison with the simpler r_A/r_B ratio previously discussed.

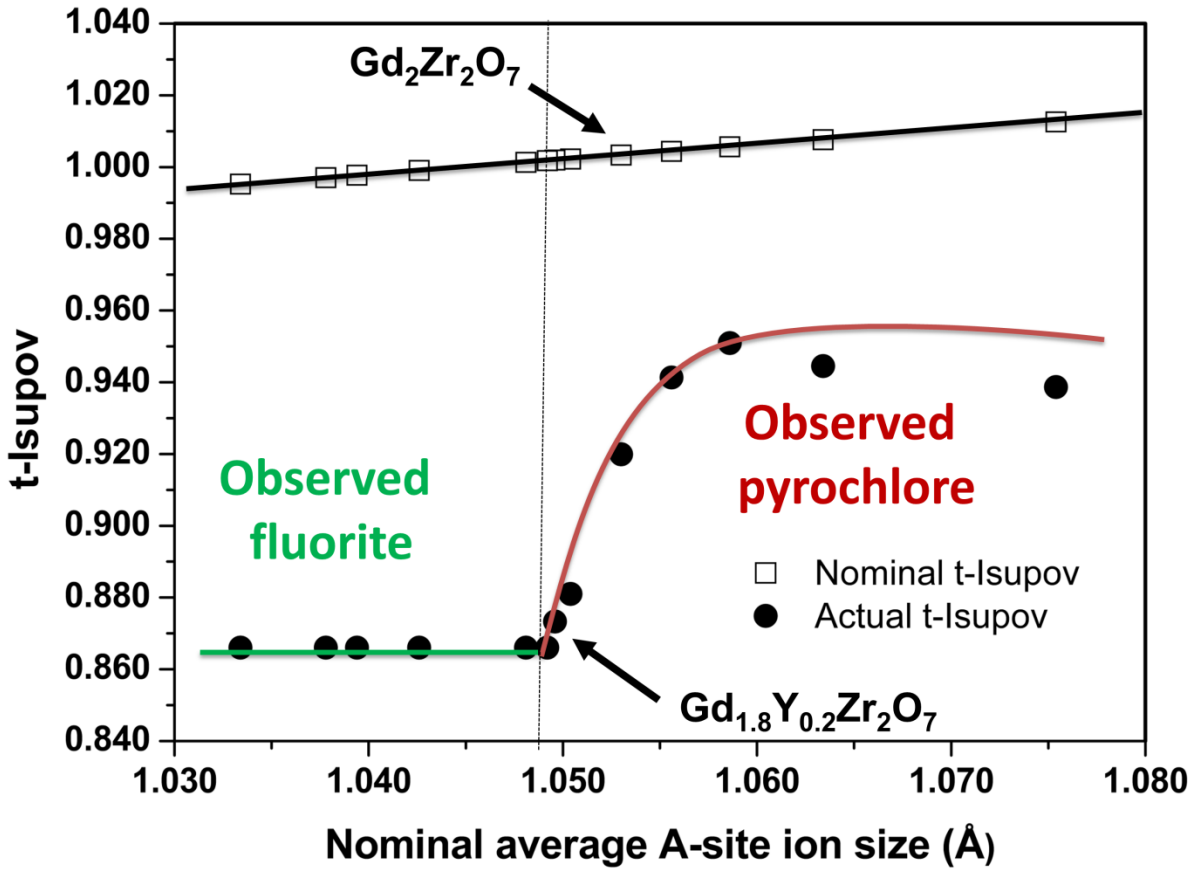

Figure 10. Isupov's [46] tolerance factor in the $Gd_{2-x}Ln_xZr_2O_7$ series, plotted as a function of the nominal (empty squares) and experimental (full circles) averaged *A*-cation size. Lines are guides for the eye.

To overcome the problem of Isupov's t_I, Cai *et al.* proposed two different tolerance factors to describe the pyrochlore crystal structure, t_1 and t_2, corresponding respectively to the A_2B_2, and

$O_{8a}A_4$ polyhedra [47]. As shown in equations [2] and [3], t_1 and t_2 depend either on the cubic unit cell parameter (a) or on the unknown oxygen positional parameter (x_{48f}) which in practice, hinders any predictive character of such factors. Furthermore, the variability and limited availability of structural information on pyrochlore compounds (in particular, the x_{48f} positional parameter), make calculations rather difficult and limit their applicability. However, some relationships were successfully established between their values and pyrochlore oxides physical properties.

$$t_1 = \frac{\left[\left(x-\frac{1}{4}\right)^2+\frac{1}{32}\right]^{\frac{1}{2}}\left(r_A+r_O\right)}{\left[\left(x-\frac{1}{2}\right)^2+\frac{1}{32}\right]^{\frac{1}{2}}\left(r_B+r_O\right)} \qquad [2]$$

$$t_2 = a\,\frac{3^{1/2}}{8\,(r_B+r_O)} \qquad [3]$$

Trying to overcome these limitations, the authors proposed the use of a mathematical relationship developed by Nikiforov to estimate the unknown x_{48f} positional parameter [48]. Worth to note, the alternative method proposed by Chakoumakos also provides suitable values of x_{48f} and could be used instead[49].

Interestingly, t_1 varies between 0.83 and 1.07 although most values are included within the 0.90 and 0.99 interval. None the less, t_2 values show a clearer trend with r_A/r_B when compared to t_1; t_2 slightly decreases with increasing r_A/r_B, whereas, t_1 is rather scattered. For a very wide range of

r_A/r_B values, both t_2 and especially t_1, are less than unity, this being a strong indication of pyrochlore structure stability.[47]

Figures 11a and 11b depict the values of both t_1 and t_2 parameters for our high-temperature annealed samples, respectively.

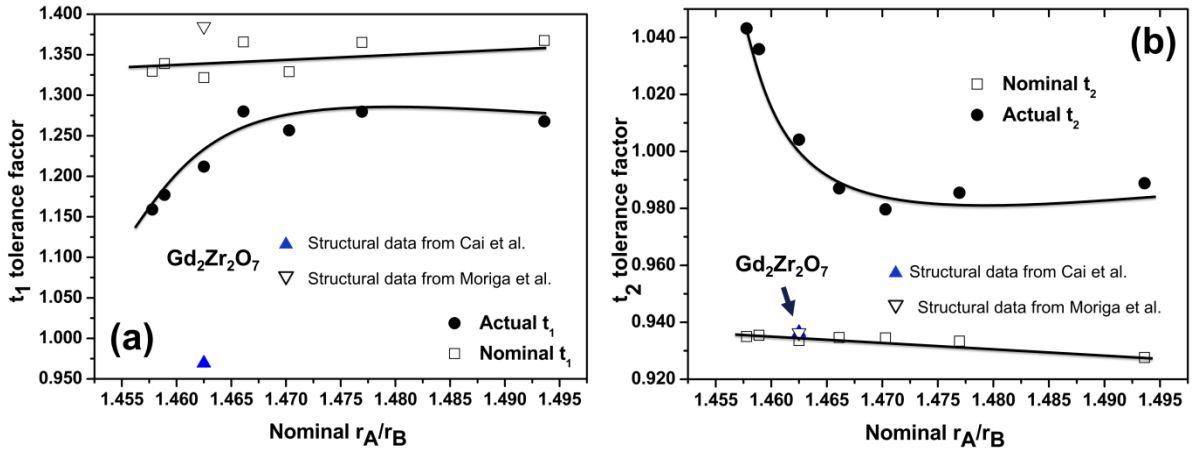

Figure 11. Cai's et al. [47] t_1 and t_2 tolerance factors in the $Gd_{2-x}Ln_xZr_2O_7$ series annealed at 1400ºC, plotted as a function of the nominal (empty squares) and experimental (full circles) averaged *A*-cation size. Down open triangles represent data form ref [50]. Lines are guides for the eye.

Some important features concerning t_1 and t_2 parameters arise from Figure 11. First, t_1 is extremely sensitive to the structural parameters used for the calculations. The values obtained for our samples series, either using the nominal populations of the A- and B-sites or using the experimental refined values, are far from the pyrochlore boundary value of t_1 proposed to be

close to unity. Furthermore, in Figure 11a we have included the t_1 values calculated for GZO using two different sets of structural parameters: *i.e.,* that given by Cai et al. [47] and a second set reported by Moriga et al. and obtained from single crystal X-ray data[50]. The value of t_1 we obtain for GZO from SXRD data is pretty close to that calculated for the latter; consequently the t_1 value obtained from Moriga *et al.* model [50] is also far from what is predicted for a pyrochlore structure. On the contrary, t_2 seems to be more robust, and the values obtained using different structural models are almost the same provided the unit cell is similar. This is because the only structural information used in Eq. [3], is the unit cell parameter. Paradoxically, the values of t_2 calculated for the Moriga et al.[50] and our structural models are pretty different, on the contrary to what happens for t_1. This is due to the different degree of inversion and cell parameters of both samples: being of 5% and 12.5227 Å,[50] respectively, for the former whereas for our sample a degree of inversion of 14% and a cell dimension of 10.4917 Å are observed. Therefore, on the contrary to what stated in ref. [47] the actual values of tolerance factors are strongly dependent on the synthesis conditions.

In any case, both tolerance factors have little, or even no, predictive capacity since their variation along the series (as a function of r_A/r_B) is smooth with no evidence near the transition from pyrochlore-to-fluorite structures, when nominal A- and B-sites occupancies, are used. On the contrary, when the experimental metal distribution is used, both t_1 and t_2 show clear evidence near the transition. Thus, t_1 is almost constant in a wide r_A/r_B region but start decreasing rapidly when this ratio approaches a value of *ca.* 1.457. Even a stronger suggestion of the phase transition is given by t_2; its value is close (lower) than unity for most samples but in the vicinity of the structural change, its value strongly rises above unity. In any case, these tolerance factors

seem to give some useful information only when real structural models are used; therefore, their predictive capacity is at least doubtful.

More recently Mouta *et al.* defined an empirical tolerance factor for compounds with pyrochlore structure based only on the ionic radii of the constituent ions and proposed its correlation with structural and physical properties [51]. The expression, given in Eq. [4] was derived by a statistical treatment of available structural data but no structural parameters are explicitly used;

$$t_{new} = 1.43373 - 0.42931\ [(r_A + r_O) / (r_B + r_O)] \qquad [4]$$

where r_A, r_B and r_O are the size of the A, B and oxygen ions, respectively.

These authors also proposed an empirical formula to calculate the unit cell parameter.

Pyrochlore distribution according to the new tolerance factor behaves as a normally distributed population, whose center occurs at a value of $t_{new} = 0.913$. For pyrochlore oxides with values close to this one, the radii ratio r_A/r_B is *ca.* 1.6. No pyrochlore is reported with a value of t_{new} higher than unity, the highest value corresponding to $Pr_2Te_2O_7$ ($t_{new} = 0.97592$) due to the lone pair of Te^{4+} ions.

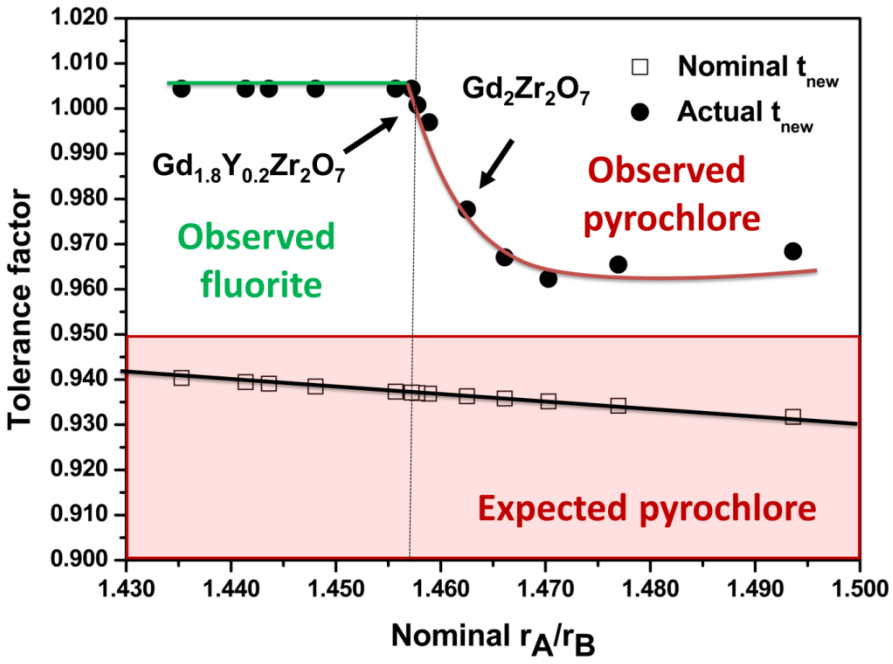

Figure 12. Mouta's et al. [51] t_{new} tolerance factor in the $Gd_{2-x}Ln_xZr_2O_7$ series, plotted as a function of the nominal (empty squares) and experimental (full circles) averaged *A*-cation size. Lines are guides for the eye.

By applying Eq. [4] to the r_A and r_B determined assuming nominal distributions at the A- and B-sites, all the our oxides heated at 1400ºC should by pyrochlore-like. However, this is not what we observed since many of them do not present long-range pyrochlore ordering, though Raman spectroscopy suggests that most of them are short-range ordered.

As for other tolerance factors discussed above, the use of the actual (experimentally determined metal distribution) gives more meaningful values. Thus, as observed in Figure 12, the values of t_{new} are close, but lower than unity, in a wide range of ionic radii ratio r_A/r_B; but clearly increases for compounds located near to the boundary between the pyrochlore and fluorite stability fields.

For a ratio r_A/r_B about 1.457, the t_{new} factor becomes slightly higher than unity and the compound adopts the fluorite structure. Thus, $t_{new} \geq 1$ seems to be a clear criterion when predicting the relative stability of the fluorite and pyrochlore structures for a specific compound.

It must be stressed that none of the discussed tolerance factors for pyrochlore oxides provides a simple, useful, convenient and sufficiently robust criterion to predict whether a given compound will present the pyrochlore or the fluorite structure. In many cases the limitation arises as a result of a more or less important degree of inversion in the occupancies of A- and B-sites of the pyrochlore structure. When a non-negligible amount of these anti-site defects are present, the experimental averaged r_A and r_B values can be significantly different from the nominal ones. Since all the tolerance factors use the nominal radii, the calculated values will have a limited predictive capability and provide poor descriptions of real materials. Probably the most robust and simplest criterion is the cation radii ratio r_A/r_B. As shown in Figure 9, the border between the pyrochlore and fluorite stability fields predicted by this radii ratio using nominal and experimental cation distributions differs only slightly being 1.460 and 1.457, respectively (less than 0.2%). The success of this very simple criterion seems to rest in the fact that it implicitly contains information about the tendency of a given pair of A and B ions to order (the higher r_A/r_B the stronger the driving force for ordering), providing a simple but powerful and robust criterion which takes into account a key feature of the pyrochlore structure such as the existence of anti-site defects. Finally, it is worth commenting that probably because of this tendency to disorder of the pyrochlore structure, it is not possible to define for pyrochlore oxides a tolerance factor as robust, meaningful and useful as the Goldschmidt factor of perovskites.

CONCLUSIONS

This paper contributes towards a better understanding of the fundamental aspects controlling the formation and annihilation of defects in the $A_2B_2O_7$ pyrochlore structure. For that purpose, we synthesized by a mechanically-induced chemical reaction various $Gd_2Zr_2O_7$-based materials for which Gd is replaced by different lanthanides. By combining XRD and Raman spectroscopy, we obtained the structural and microstructural features of the as-prepared samples and showed that they are all *fluorite*-like materials, even after firing at 800°C; upon firing at higher temperatures (1400°C), all but $Gd_{1.20}Y_{0.80}Zr_2O_7$ undergo a phase transition to *pyrochlore*-like structures showing different degrees of disorder as a function of the type and amount of the substituted lanthanide. Using the structural data, we have also tested various metrics or criteria proposed in the literature for predicting the formation and stability of the pyrochlore structure. We conclude that none of the criteria, except the simple radius ratio rule (r_A/r_B), are predictive. Any attempt to propose an empirical index for pyrochlore oxides, similar to the Goldschmidt *tolerance factor*, is hampered by the intrinsic tendency of this structure-type to accept cation anti-site defects. Moreover, nominal and experimental averaged r_A and r_B values in any specific material can be significantly different when a non-negligible amount of these defects are present. The success of the radius ratio rule is probably due to the fact that it implicitly contains information about the tendency of a given pair of A- and B-site cations to order or disorder; the boundary between the pyrochlore and fluorite stability fields predicted by this rule using nominal and experimental cation distributions, differs only slightly, 1.460 vs. 1.457, respectively (less than 0.2%).

ASSOCIATED CONTENT

Supporting Information.

Tables SI 1 and SI 2: final structural and microstructural parameters of $Gd_{2-x}Ln_xZr_2O_7$ samples prepared by mechanical milling and post-milling thermal treatment at 800ºC and 1400ºC. Figure SI 1: enlargement of the XRD patterns of the end members of the $Gd_{2-x}Ln_xZr_2O_7$ series at the position of the (111) fluorite sub-structure peak showing slight broadening.

AUTHOR INFORMATION

Corresponding Author

E-mail: uamador@ceu.es

AKNOWLEDGEMENTS

This work was financially supported by CONACYT (Mexico, Grant CB2013-01-221701) and MINECO (Spain, project MAT2016- 78362-C4-1-R). UA acknowledges financial support by USPCEU through the SAIDRXMEB laboratory. RCE and ML acknowledge supported by the Energy Frontier Research Center *Materials Science of Actinides* funded by the US Department of Energy, Office of Science, Office of Basic Energy Sciences (DE-SC0001089). Portions of this work were performed at HPCAT (Sector 16), Advanced Photon Source, Argonne National Laboratory. HPCAT operations are supported by DOE-NNSA under award No. DE-NA0001974 and DOE-BES under award No. DE-FG02-99ER45775, with partial instrumentation funding by NSF. APS is supported by DOE-BES, under contract No. DE-AC02-06CH11357. Beamtime was

obtained through support from the U.S. Department of Energy (DOE) National Nuclear Security Administration (NNSA) through the Carnegie DOE Alliance Center (CDAC) under grant number DE-NA-0002006.

REFERENCES

1. Wuensch, B. J.; Eberman, K. W.; Heremans, C.; Ku, E. M.; Onnerud, P.; Yeo, E. M. E.; Haile, S. M.; Stalick, J. K.; Jorgensen, J. D. Connection between oxygen-ion conductivity of pyrochlore fuel-cell materials and structural change with composition and temperature. *Solid State Ionics* **2000,** 129, 111-133.

2. Vassen, R.; Jarligo, M. O.; Steinke, T.; Mack, D. E.; Stoever, D. Overview on advanced thermal barrier coatings. *Surf. Coat. Technol.* **2010,** 205, 938-942.

3. Feng, J.; Xiao, B.; Wan, C. L.; Qu, Z. X.; Huang, Z. C.; Chen, J. C.; Zhou, R.; Pan, W. Electronic structure, mechanical properties and thermal conductivity of Ln(2)Zr(2)O(7) (Ln = La, Pr, Nd, Sm, Eu and Gd) pyrochlore. *Acta Mater.* **2011,** 59, 1742-1760.

4. Lang, M.; Zhang, F.; Zhang, J.; Wang, J.; Lian, J.; Weber, W. J.; Schuster, B.; Trautmann, C.; Neumann, R.; Ewing, R. C. Review of A(2)B(2)O(7) pyrochlore response to irradiation and pressure. *Nucl. Instrum. Methods Phys. Res., Sect. B* **2010,** 268, 2951-2959.

5. Schelling, P. K.; Phillpot, S. R.; Grimes, R. W. Optimum pyrochlore compositions for low thermal conductivity. *Philos. Mag. Lett.* **2004,** 84, 127-137.

6. Martel, L.; Naji, M.; Popa, K.; Vigier, J.-F.; Somers, J. Fingerprint of local disorder in long range ordered isometric pyrochlores. *Sci. Rep.* **2017,** 7, 12269.

7. Simeone, D.; Thorogood, G. J.; Huo, D.; Luneville, L.; Baldinozzi, G.; Petricek, V.; Porcher, F.; Ribis, J.; Mazerolles, L.; Largeau, L.; Berar, J. F.; Surble, S. Intricate disorder in defect fluorite/pyrochlore: a concord of chemistry and crystallography. *Sci. Rep.* **2017,** 7, 3727.

8. Hagiwara, T.; Nomura, K.; Kageyama, H. Crystal structure analysis of Ln(2)Zr(2)O(7) (Ln = Eu and La) with a pyrochlore composition by high-temperature powder X-ray diffraction. *J. Ceram. Soc. Jpn.* **2017,** 125, 65-70.

9. Shamblin, J.; Feygenson, M.; Neuefeind, J.; Tracy, C. L.; Zhang, F.; Finkeldei, S.; Bosbach, D.; Zhou, H.; Ewing, R. C.; Lang, M. Probing disorder in isometric pyrochlore and related complex oxides. *Nat. Mater.* **2016,** 15, 507.

10. Heremans, C.; Wuensch, B. J.; Stalick, J. K.; Prince, E. Fast-ion conducting Y-2(ZryTi1-y)(2)O-7 pyrochlores - neutron rietveld analysis of disorder-induced by Zr substitution. *J. Solid State Chem.* **1995,** 117, 108-121.

11. Liu, Y.; Withers, R. L.; Noren, L. The pyrochlore to 'defect fluorite' transition in the Y-2(ZryTi1-(y))(2)O-7 system and its underlying crystal chemistry. *J. Solid State Chem.* **2004,** 177, 4404-4412.

12. Mandal, B. P.; Krishna, P. S. R.; Tyagi, A. K. Order-disorder transition in the Nd2-yYyZr2O7 system: Probed by X-ray diffraction and Raman spectroscopy. *J. Solid State Chem.* **2010,** 183, 41-45.

13. Blanchard, P. E. R.; Liu, S.; Kennedy, B. J.; Ling, C. D.; Zhang, Z.; Avdeev, M.; Cowie, B. C. C.; Thomsen, L.; Jang, L.-Y. Investigating the order-disorder phase transition in Nd2-xYxZr2O7 via diffraction and spectroscopy. *Dalton Trans.* **2013,** 42, 14875-14882.

14. Withers, R. L.; Welberry, T. R.; Larsson, A. K.; Liu, Y.; Noren, L.; Rundlof, H.; Brink, F. J. Local crystal chemistry, induced strain and short range order in the cubic pyrochlore (Bi1.5-alpha Zn0.5-beta)(Zn0.5-gamma Nb1.5-delta)O(7-1.5 alpha-beta-gamma-2.5-delta) (BZN). *J. Solid State Chem.* **2004,** 177, 231-244.

15. Minervini, L.; Grimes, R. W.; Tabira, Y.; Withers, R. L.; Sickafus, K. E. The oxygen positional parameter in pyrochlores and its dependence on disorder. *Philos. Mag. A* **2002,** 82, 123-135.

16. Blanchard, P. E. R.; Clements, R.; Kennedy, B. J.; Ling, C. D.; Reynolds, E.; Avdeev, M.; Stampfl, A. P. J.; Zhang, Z.; Jang, L.-Y. Does Local Disorder Occur in the Pyrochlore Zirconates? *Inorg. Chem.* **2012,** 51, 13237-13244.

17. Bellier-Castella, L.; Gingras, M. J.; Holdsworth, P. C.; Moessner, R. Frustrated order by disorder: The pyrochlore anti-ferromagnet with bond disorder. *Can. J. of Phys.* **2001,** 79, 1365-1371.

18. Vanderah, T. A.; Levin, I.; Lufaso, M. W. An unexpected crystal-chemical principle for the pyrochlore structure. *Eur. J. Inorg. Chem.* **2005,** 14, 2895-2901.

19. Subramanian, M. A.; Aravamudan, G.; Rao, G. V. S. Oxide Pyrochlores - a Review. *Prog. Solid State Chem.* **1983,** 15, 55-143.

20. Vandijk, T.; Devries, K. J.; Burggraaf, A. J. Electrical-conductivity of fluorite and pyrochlore GdxZr1-xO2-x/2 NdxZr1-xO2-x/2 solid-solutions. *Phys. Status Solidi A* **1980,** 58, 115-125.

21. Diaz-Guillen, J. A.; Fuentes, A. F.; Diaz-Guillen, M. R.; Almanza, J. M.; Santamaria, J.; Leon, C. The effect of homovalent A-site substitutions on the ionic conductivity of pyrochlore-type Gd2Zr2O7. *J. Power Sources* **2009,** 186, 349-352.

22. Wu, J.; Wei, X. Z.; Padture, N. P.; Klemens, P. G.; Gell, M.; Garcia, E.; Miranzo, P.; Osendi, M. I. Low-thermal-conductivity rare-earth zirconates for potential thermal-barrier-coating applications. *J. Am. Ceram. Soc.* **2002,** 85, 3031-3035.

23. Diaz-Guillen, J. A.; Dura, O. J.; Diaz-Guillen, M. R.; Bauer, E.; Lopez de la Torre, M. A.; Fuentes, A. F. Thermophysical properties of Gd2Zr2O7 powders prepared by mechanical milling: Effect of homovalent Gd3+ substitution. *J. Alloys Compd.* **2015,** 649, 1145-1150.

24. Wang, S. X.; Begg, B. D.; Wang, L. M.; Ewing, R. C.; Weber, W. J.; Kutty, K. V. G. Radiation stability of gadolinium zirconate: A waste form for plutonium disposition. *J. Mater. Res.* **1999,** 14, 4470-4473.

25. Lang, M.; Zhang, F. X.; Ewing, R. C.; Lian, J.; Trautmann, C.; Wang, Z. Structural modifications of Gd(2)Zr(2-x)Ti(x)O(7) pyrochlore induced by swift heavy ions: Disordering and amorphization. *J. Mater. Res.* **2009,** 24, 1322-1334.

26. Huot, J.; Ravnsbaek, D. B.; Zhang, J.; Cuevas, F.; Latroche, M.; Jensen, T. R. Mechanochemical synthesis of hydrogen storage materials. *Prog. Mater. Sci.* **2013,** 58, 30-75.
27. Friscic, T. New opportunities for materials synthesis using mechanochemistry. *J. Mater. Chem.* **2010,** 20, 7599-7605.
28. Dreizin, E. L.; Schoenitz, M. Mechanochemically prepared reactive and energetic materials: a review. *J. Mater. Sci.* **2017,** 52, 11789-11809.
29. Fuentes, A. F.; Takacs, L. Preparation of multicomponent oxides by mechanochemical methods. *J. Mater. Sci.* **2013,** 48, 598-611.
30. Hammersley, A. *Computer Program Fit 2D*, Grenoble, France, 1998.
31. Rodriguez Carvajal, J. Recent advances in magnetic-structure determination by neutron powder diffraction. *Physica B* **1993,** 192, 55-69.
32. Langford, J. I. *NIST Special Publication 846. Proceedings of the International Conference "Accuracy in Powder Diffraction II"*. Gaithersburg, MD, USA,, 1992.
33. Langford, J. I. *Defect and Microstructure Analysis by Diffraction*. Oxford University Press: Oxford, U.K., 1999.
34. Halder, N. C.; Wagner, C. N. J. Separation of particle size and lattice strain in integral breadth measurements. *Acta Crystallogr., Sect. A* **1966,** 20, 312.
35. Louër, D. *Defect and Microstructure Analysis by Diffraction*. Oxford University Press: Oxford, U.K., 1999.
36. Shannon, R. Revised effective ionic radii and systematic studies of interatomic distances in halides and chalcogenides. *Acta Crystallogr., Sect. A* **1976,** 32, 751-767.
37. Moreno, K. J.; Fuentes, A. F.; Maczka, M.; Hanuza, J.; Amador, U.; Santamaria, J.; Leon, C. Influence of thermally induced oxygen order on mobile ion dynamics in Gd-2(Ti0.65Zr0.35)(2)O-7. *Phys. Rev. B* **2007,** 75, 184303.
38. Hess, N. J.; Begg, B. D.; Conradson, S. D.; McCready, D. E.; Gassman, P. L.; Weber, W. J. Spectroscopic investigations of the structural phase transition in Gd2(Ti1-yZry)(2)O-7 pyrochlores. *J. Phys. Chem. B* **2002,** 106, 4663-4677.
39. Tracy, C. L.; Shamblin, J.; Park, S.; Zhang, F. X.; Trautmann, C.; Lang, M.; Ewing, R. C. Role of composition, bond covalency, and short-range order in the disordering of stannate pyrochlores by swift heavy ion irradiation. *Phys. Rev. B* **2016,** 94, 064102.
40. Shamblin, J.; Tracy, C. L.; Palomares, R. I.; O'Quinn, E. C.; Ewing, R. C.; Neuefeind, J.; Feygenson, M.; Behrens, J.; Trautmann, C.; Lang, M. Similar local order in disordered fluorite and aperiodic pyrochlore structures. *Acta Mater.* **2018,** 144, 60-67.
41. Glerup, M.; Nielsen, O. F.; Poulsen, F. W. The structural transformation from the pyrochlore structure, A(2)B(2)O(7), to the fluorite structure, AO(2), studied by Raman spectroscopy and defect chemistry modeling. *J. Solid State Chem.* **2001,** 160, 25-32.
42. Moreno, K. J.; Fuentes, A. F.; Maczka, M.; Hanuza, J.; Amador, U. Structural manipulation of pyrochlores: Thermal evolution of metastable Gd-2(Ti1-yZry)(2)O-7 powders prepared by mechanical milling. *J. Solid State Chem.* **2006,** 179, 3805-3813.
43. Xia, X.-L.; Ouyang, J.-H.; Liu, Z.-G. Electrical Properties of Gadolinium-Europium Zirconate Ceramics. *J. Am. Ceram. Soc.* **2010,** 93, 1074-1080.
44. Mandal, B. P.; Pandey, M.; Tyagi, A. K. Gd2Zr2O7 pyrochlore Potential host matrix for some constituents of thoria based reactor's waste. *J. Nucl. Mater.* **2010,** 406, 238-243.
45. Balzar, D.; Popovic, S. Reliability of the Simplified Integral-Breadth Methods in Diffraction Line-Broadening Analysis. *J. Appl. Crystallogr.* **1996,** 29, 16-23.

46. Isupov, V. A. Geometric criteria of structures of the pyrochlore type. *Kristallografiya* **1958,** 3, 99-100.
47. Cai, L.; Arias, A. L.; Nino, J. C. The tolerance factors of the pyrochlore crystal structure. *J. Mater. Chem.* **2011,** 21, 3611-3618.
48. Nikiforov, L. G. Possible method for estimating x-parameter in pyrochlor-type compounds with general formula A2B2O7. *Kristallografiya* **1972,** 17, 408.
49. Chakoumakos, B. C. Systematics of the pyrochlore structure type, ideal A2B2X6Y. *J. Solid State Chem.* **1984,** 53, 120-129.
50. Moriga, T.; Yoshiasa, A.; Kanamaru, F.; Koto, K.; Yoshimura, M.; Somiya, S. Crystal-structure analyses of the pyrochlore-type and fluorite-type Zr2Gd2O7 and anti-phase domain-structure. *Solid State Ionics* **1989,** 31, 319-328
51. Mouta, R.; Silva, R. X.; Paschoal, C. W. A. Tolerance factor for pyrochlores and related structures. *Acta Crystallogr., Sect. B* **2013,** 69, 439-445.

For Table of Contents Only

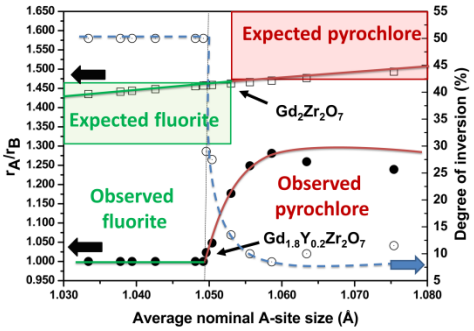

TOC

Synopsis: Various indices proposed for predicting the formation of the pyrochlore structure are tested. None of them, except the simple radius ratio rule (r_A/r_B), is predictive. Its success is probably due to the fact that it implicitly contains information about the tendency of a given pair of A- and B-site cations to order or disorder; which is of paramount importance in pyrochlore oxides since this structure-type is prone to accommodate large degrees of cation anti-site defects.